SIMULATION OF THE INTENSITY AND POLARIZATION OF SKYLIGHT DURING TWILIGHT PERIOD

Wu Beiying (吴北婴) and *Lu Daren* (吕达仁)

Institute of Atmospheric Physics, Academia Sinica, Beijing

Received September 19, 1986

ABSTRACT

Monte-Carlo method is applied to simulate the intensities and degrees of polarization in twilight sky after the eruption of the El Chichon volcano and during the 1977 volcanically quiet period, respectively. The results coincide well with the observations. It is found that the significance of multiple scattering is completely different in these two periods; the background concentration of stratospheric aerosols has probably increased since the 1960's. It is necessary to study the cause of the increase and its impact on climate.

I. INTRODUCTION

In recent years, much attention has been paid to the possible influence of stratospheric aerosols on the radiation budget and on stratospheric dynamics and climate. Therefore, the detection of stratospheric aerosols has become a main focus of atmospheric research. Compared with other detection methods, one of the earliest but still useful method is the inference of characteristics of stratospheric aerosols from the intensity and polarization of skylight during the twilight period with a photometer on the ground. This method is welcomed in several aspects: The instrument is relatively simple and observations can be made continuously; the sampling space is large and the sensor itself does not disturb the observed objects. Therefore, this method has been used extensively to study stratospheric aerosols since Arago observed the polarization of skylight by this method in 1809. Although a wealth of observation data have been accumulated, there are some difficulties in explaining them. Limited by the accuracy and the time constant of the instrument, most of the researchers in the past only detected polarization or neutral point of skylight. Observations were conducted in different ways and there were no simultaneous measurements of aerosols available. The essential difficulty, however, is that there is hardly any analysis of the data using a complete theoretical model. The reason is that the radiative transfer equation under twilight condition is difficult to solve by ordinary approaches, except the time-consuming Monte-Carlo method. Therefore, most researchers in this field adopt the approximation of single or double scattering (e.g. Dave, 1956; Divari, 1967; Steinhorst, 1977) or neglect aerosols (Blattner et al., 1974). Among them Steinhorst has done notable work by establishing a second-order scattering model, conducting a set of observations and especially proposing a scheme to retrieve the optical depth and size distribution of stratospheric aerosols from the near-infrared data. But as mentioned above, these approximations are valid only for specific detecting schemes and can not be generally used. Since atmospheric conditions, wavelengths and detecting directions vary in different detecting schemes, the fractions of higher-order scattering in total scattering intensity would change too. The effect of the aerosol concentration, size distribution and refractive

index on skylight would also change. In fact, non of these problems can be thoroughly solved with a simplified model. Therefore, based on the work of Collins et al. (1971), we have established a backward Monte-Carlo computational code which can solve the radiation transfer equation in spherically-layered atmosphere. Processes such as the Rayleigh and aerosol multiple scattering, aerosol and O_3 absorption, atmospheric refraction and the surface reflection can easily be incorporated in the present code. The detecting wavelength, direction and the solar zenith angle can be changed. The calculation procedure will be described in another paper. This paper presents primarily a simulation of the intensity and degree of polarization of 0.7 μm wavelength twilight in local zenith direction in two typical cases. One is after the eruption of the El Chichon volcano in 1982, the other is in the spring of 1977 which is referred to a 'quiet' background period. The simulation of skylight after the volcanic eruption is first presented and then the background period. The selections of the parameters in these two cases are described separately.

II. SIMULATION OF SKYLIGHT AFTER VOLCANIC ERUPTION

The volcanic cloud produced by the April 1982 eruption of the El Chichon is the most massive one to cover the Northern Hemisphere in the last 70 years. The optical depth reached 10^{-1} in the Northern Tropics during its first six month. Such an optical depth is large enough to disturb the earth's and the atmospheric radiation budget and the climate. Therefore, many scientists detected various characteristics of the volcanic cloud during and after the eruption. The researchers at Mauna Loa Observatory observed both the intensity and polarization of skylight during the twilight period with a photometer and the volcanic aerosols with a lidar (Coulson, 1983). These observations were superior to many other observations done previously in both terms of accuracy and completeness. But there were some difficulties in the explanation of the abnormality in the measured intensity and polarization. Our Monte-Carlo code is suitable for such a purpose. Therefore, we simulated the intensity and degree of polarization at 0.7 μm wavelength in local zenith direction using the data from Mauna Loa on June 22, 1982. In the following sections, the model atmosphere will be described and then the simulated results will be analyzed and discussed.

1. *Computation Procedure and the Model Atmosphere*

The model spherically-layered atmosphere is composed of N layers of aerosol-bearing air. Optical properties such as the Rayleigh scattering coefficient, aerosol scattering coefficient, O_3 absorption coefficient, and atmospheric refractive index in each layer are homogeneous. The surface is a Lambertian surface with albedo A. The Rayleigh scattering coefficient and atmospheric refractive index are calculated according to the U.S. Standard Atmosphere, 1976. Elterman's table is adopted for calculating the O_3 absorption coefficient (Elterman, 1968), and the refractive index of aerosols is assumed to be $1.45-0.00i$ because it is generally accepted that the stratospheric aerosol consists of liquid droplets with 75% H_2SO_4 and 25% water (Hamill et al., 1977).

The aerosol scattering coefficient is determined in the following way:

(i) Below 11 km, the coefficient is calculated by the method given in the Handbook of Geophysics and Space Environments.

(ii) Above 11 km, the coefficient is deduced from lidar data (DeLuisi et al., 1985). The aerosol backscattering ratio R measured by lidar is

$$R=\sigma_{\pi M}/\sigma_{\pi R}, \tag{1}$$

where $\sigma_{\pi R}$ and $\sigma_{\pi M}$ are the Rayleigh and aerosol backscattering coefficients, respectively. Thus the aerosol scattering coefficient is

$$\sigma_{SM}=\frac{\sigma_{\pi R}\cdot R}{P_M(\pi)}=\frac{3}{8\pi}\frac{\sigma_{SR}\cdot R}{P_M(\pi)}, \tag{2}$$

where σ_{SR} and σ_{SM} are the Rayleigh and aerosol scattering coefficients, respectively, and $P_M(\pi)$ is the aerosol phase function. Since no aerosol absorption is taken into account, the reciprocal of $P_M(\pi)$ is equivalent to the so-called extinction-to-backscatter ratio.

The selection of the aerosol size distribution is somewhat arbitrary because of no *in situ* measurements being available. There are two effects of the size distribution on the simulation: 1) The difference in the phase function would result in different scattered intensities in the same direction. 2) The aerosol scattering coefficient deduced through Eq. (2) will change as $P_M(\pi)$ changes. It is shown from the simulations that the latter effect is more serious than the former one.

We determine the phase function and extinction-to-backscatter ratio separately. Aerosol scattering phase functions and profiles of the aerosol scattering coefficients corresponding to a number of aerosol size distributions are calculated. Then the degrees of polarization of skylight in local zenith direction are simulated corresponding to each combination of one phase function with one aerosol scattering profile at solar zenith angles $\theta=94.8°$ (where the polarization is more sensitive to changes in contents of stratospheric aerosols) and $\theta=88.0°$ (where the polarization is more sensitive to the aerosol optical depth of the whole vertical column). The results are compared with the measured polarization. Finally, the phase function of the AFGL size distribution with a mode radius $r_c=0.10$ μm and a extinction-to-backscatter ratio of 39.4 are selected. The optical depth of atmospheric columnar aerosol thus obtained is 0.412, the optical depth of the aerosols above 11 km is 0.216 and the total optical depth is 0.460.

2. *Results and Analysis*

The calculated polarization and intensity of skylight for local zenith with solar zenith angles ranging from 88° to 96° are shown in Figs. 1 and 2. The results reasonably coincide with the observations. It follows that the present procedure is applicable. But some important features should be pointed out.

(1) *The effect of multiple scattering*

Based on the observations during the spring of 1977, Coulson (1980) suggested that primary scattering plays a major role at the 0.7 μm wavelength for zenith detecting. But the present results show that this inference cannot be applied to the period after the El Chichon eruption. Shown in Table 1 is the ratio of the scattered intensities of various orders to the first-order scattering and in Table 2 is the ratio of the degrees of polarization of various orders weighted by intensity to the degree of polarization of the first-order scattering. Shown in Fig. 3 and Fig. 4 are curves corresponding to Table 1 and Table 2, respectively. The significance of higher order scattering in both intensity and polarization is obvious. In the case of $88° < \theta < 94.8°$, the intensities of the second- and the third-order scattering are almost equal to that of the first-order scattering. The sum of the intensities of the two is obviously greater than the intensity of the first-order scattering. Therefore, it is not appropriate to neglect the second- and the third-order scattering. The intensities of

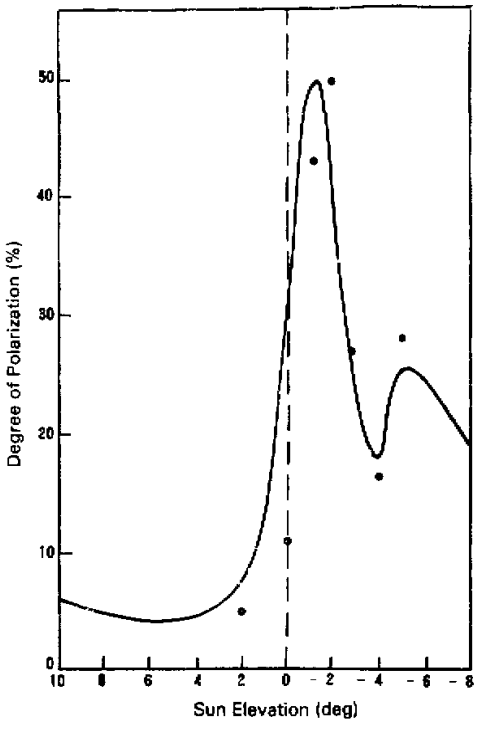

Fig. 1. The zenith polarization. Solid line is the observation; the dots are the simulation.

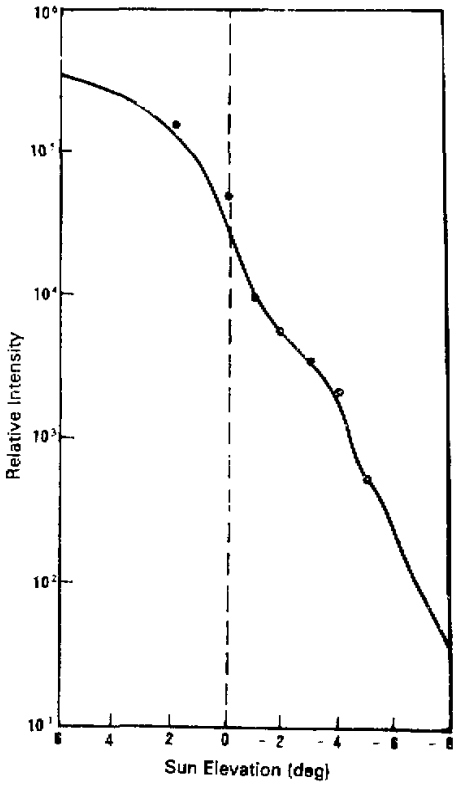

Fig. 2. The zenith intensity. The meaning of the symbols are the same as in Fig. 1.

Table 1. The Ratio of the Scattered Intensities of Various Orders to the First-order Scattering. τ is the total optical depth, θ and θ' are the true and apparent zenith angles of the sun, respectively. The detecting zenith angle is 0° and the wavelength is 0.7 μm.

τ	θ	θ'	1	2/1	3/1	4/1	5/1	6/1	7/1	8/1
.460	88.0	88.0	1.00	1.07	.76	.21	.07	.04	.01	.00
.460	90.0	90.0	1.00	.90	.94	.22	.08	.08	.04	.00
.460	92.0	91.3	1.00	1.05	.95	.52	.15	.11	.15	.00
.460	92.6	91.9	1.00	.77	.81	.51	.15	.09	.15	.00
.460	93.9	93.0	1.00	.83	.53	.27	.13	.08	.15	.00
.460	94.8	94.0	1.00	1.20	.74	.40	.18	.10	.21	.00
.460	95.9	95.0	1.00	76.0	87.0	44.5	26.7	12.6	23.6	1.03

the second- and the third-order scattering for $\theta > 94.8°$ are much higher than that of the first-order scattering. Even the seventh- and the eighth-order scattering are of the same order of magnitude as the first-order scattering and should not be neglected either.

(2) *The calculated intensity*

The comparison between the calculated and measured intensities is shown in Fig. 2.

Table 2. The Ratio of the Degree of Polarization of Various Orders Weighted by Intensity to the Degree of the First-order Scattering. The detecting angle and wavelength are the same as in Table 1.

τ	θ	θ'	1	2/1	3/1	4/1	5/1	6/1	7/1	8/1
.460	88.0	88.0	1.00	.06	.69	.38	.01	.03	.01	/
.460	90.0	90.0	1.00	.41	.40	.06	.00	.05	.01	/
.460	92.0	91.3	1.00	.42	.46	.19	.05	.03	.02	/
.460	92.6	91.9	1.00	.45	.59	.18	.06	.03	.02	/
.460	93.9	93.0	1.00	1.15	2.00	.13	.20	.14	.09	/
.460	94.8	94.0	1.00	3.29	8.29	.55	.71	.45	.43	/
.460	95.9	95.0	1.00	123.	229.	11.4	13.21	7.27	13.58	/

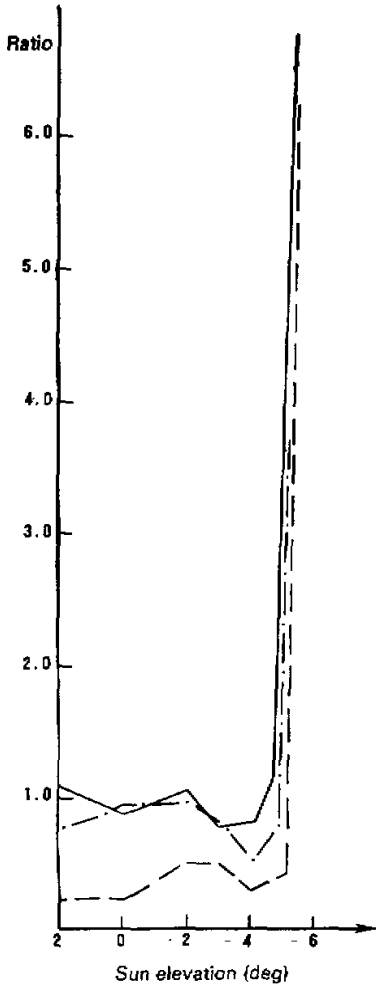

Fig. 3. Ratio of the scattered intensities of various orders to first-order intensity. — ratio of 2nd to 1st; ·—· 3rd to 1st; - - - - 4th to 1st,

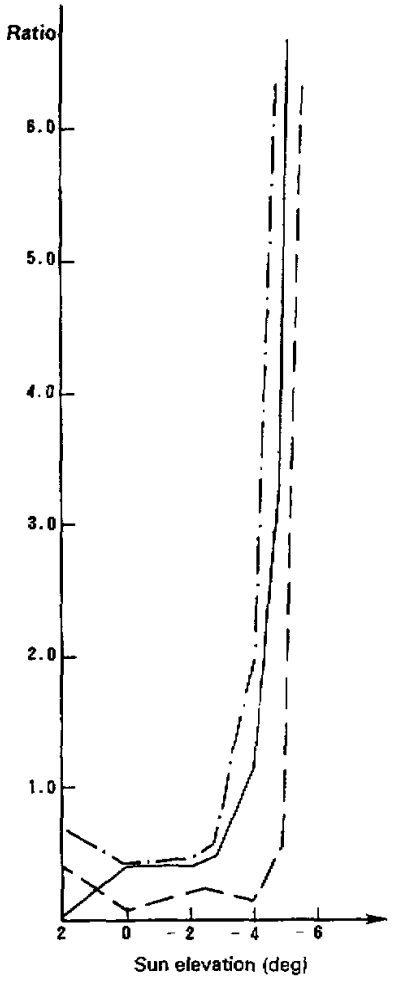

Fig. 4. Ratio of the degree of polarization of various orders weighted by intensity to the degree of polarization of the first-order, see caption for Fig. 3,

Since the measured values are in relative units, we set the calculated intensity at various solar zenith angles by assuming that the calculated intensity is equal to the measured intensity at a certain angle (92.6°). The curve coincides with the measurement quite well.

Table 3. The Intensity and Degree of Polarization at Different Surface Albedos A. The number with a minus symbol is the exponential index, e.g. '0.31−2' refers to 0.31×10^{-2}. The detecting angle and wavelength are the same as in Table 1.

τ	θ	Intensity				Polarization	
		A=0.0		A=1.0		A=0.0	A=1.0
.460	88.0	.52	−2	.72	−2	0.05	0.03
.460	90.0	.15	−2	.24	−2	0.12	0.07
.460	92.0	.27	−3	.46	−3	0.41	0.22
.460	92.6	.16	−3	.30	−3	0.49	0.26
.460	93.9	.90	−4	.12	−3	0.27	0.22
.460	94.8	.65	−4	.77	−4	0.16	0.14
.460	95.9	.14	−4	.24	−4	0.28	0.17

3. *The Effect of the Surface Albedo*

The results mentioned above are all for a black surface (A=0). Shown in Table 3 are the intensities and degrees of polarization at various values of the surface albedo. The surface albedo obviously changes the degree of polarization as well as the intensity when $\theta<92.6°$. However, the effect of the surface albedo tends to be less important for $\theta>92.6°$.

It should be pointed out that the sampling space of a lidar is smaller than that of a photometer. The scattered light detected by a photometer is an average over a very large area especially when multiple scattering plays an important role. On the other hand, the backscattering detected by a lidar comes only from the vertical column in the zenith direction. Therefore, a small difference between the two kinds of measurements is expected.

Besides, the size distribution of aerosol is assumed the same throughout the atmosphere for computation efficiency. However, the assumption may be questioned in some cases. For example, the deposition speed of the volcanic debris varies as a function of the particle size. As a result the size distribution might vary with height even in the stratosphere.

III. SIMULATION OF SKYLIGHT DURING BACKGROUND PERIOD

The period extending roughly from mid-1977 through early 1980 has been cited by several studies using several measurement techniques as a background period when the stratospheric aerosol was free from major volcanically induced increases. During the spring of 1977, Coulson (1980, 1981) performed an extensive set of measurements of the polarization and intensity of twilight in the direction of the zenith at Mauna Loa Observatory at a height of 3400 m. Reliable data were obtained on 63 different days for over 350 h of continuous measurements of skylight intensity, degree of polarization and orientation of the plane of polarization. Nine of the very clear days that occurred during the measurement period were selected as low turbidity days, and average low turbidity curves were computed from the nine sets of data. The main criterion was that the zenith polarization at sunrise should be at least 85% at $\lambda=0.80$ μm. The following sections describe the Monte-Carlo simulation of the 0.7 μm skylight intensity, degree of polarization in the zenith direction using a vertical profile of aerosol concentration derived from the measurements by Jung et al. in 1959 and

1960 with impactors (Handbook of Geophysics and Space Environments) and the comparison of the simulation with the low turbidity average data measured by Coulson in 1977 (Coulson, 1980, 1981).

1. *Selection of Parameters*

During the background period, the size distribution of stratospheric aerosols should be narrower because of the absence of larger volcanic debris. And stratospheric aerosols should play a minor role. Therefore, the standard Haze M distribution of mode radius $r_c=0.05$ μm and the aerosol refractive index $1.5-0.004i$ were selected. Two profiles of the aerosol scattering coefficients were used: Profile (A) is calculated exactly according to Handbook of Geophysics and Space Environments which was based on the measurements by Junge et al. during 1959–1960; profile (B) is the same as profile (A) except that the coefficients above 15 km is increased by a factor of 10.

2. *Results and Analysis*

(1) *The effect of multiple scattering*

Shown in Table 4 and Table 5 are the ratios of the scattered intensities of various orders to the first-order scattered intensity corresponding to profiles (A) and (B), respectively. Figures 5 and 6 are the curves corresponding to Tables 4 and 5, respectively. It is obvious that the first-order scattering dominates in this case. The maximum intensity of the second-order scattering is only about 9 percent of the first-order (at a solar zenith angle of 86°). The third-order scattered intensity is only about 3% of the first-order one. As an approximation, the second- and the third-order scattering are negligible. This is consistent with Coulson's assertion but completely different from the situation after the eruption of the El Chichon.

Table 4. The Ratio of the Scattered Intensities of Various Orders to the First-order Scattering for Profile (A). τ is the total optical depth, θ and θ' are the true and apparent zenith angles of the sun, respectively. The detecting zenith angle is 0° and the wavelength is 0.7 μm.

τ	θ	θ'	1	2/1	3/1	4/1	5/1	6/1
.210	86.0	86.0	1.00	.090	.031	.008	.002	.000
.210	88.0	88.0	1.00	.074	.027	.005	.001	.000
.210	90.0	90.0	1.00	.051	.018	.002	.000	.000
.210	92.6	91.9	1.00	.015	.006	.002	.000	.000
.210	93.9	93.0	1.00	.017	.002	.002	.000	.000
.210	95.3	94.3	1.00	.019	.001	.012	.000	.000
.210	95.9	95.0	1.00	.031	.000	.028	.000	.000

Table 5. The Ratio of the Scattered Intensities of Various Orders to the First-order Scattering for Profile (B). The detecting angle and wavelength are the same as in Table 4.

τ	θ	θ'	1	2/1	3/1	4/1	5/1	6/1
.215	86.0	86.0	1.00	.092	.026	.007	.001	.000
.215	88.0	88.0	1.00	.076	.020	.005	.001	.000
.215	90.0	90.0	1.00	.051	.012	.002	.001	.000
.215	92.6	91.9	1.00	.030	.014	.000	.000	.000
.215	93.9	93.0	1.00	.033	.016	.001	.000	.000
.215	95.3	94.3	1.00	.044	.009	.000	.000	.000

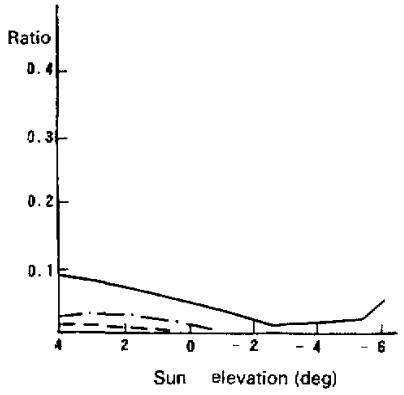

Fig. 5. Ratio of the scattered intensities of various orders to the first-order intensity for profile (A). See caption for Fig. 3.

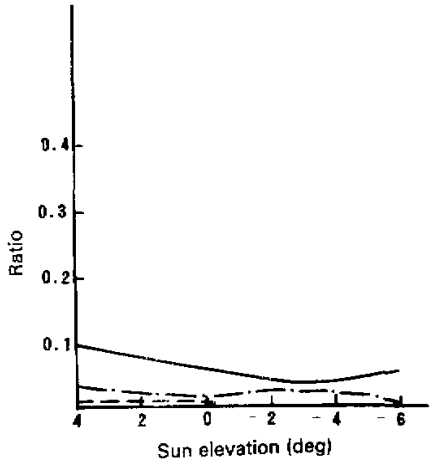

Fig. 6. Ratio of the scattered intensities of various orders to the first-order intensity for profile (B). See caption for Fig. 3.

(2) *Contributing regions*

In order to identify the location of regions where aerosols contribute most effectively to the measurements (we call the regions contributing regions), we calculated the average height of the points at which scatterings take place. As mentioned in III 2 (1), the first-order scattering dominates in the background period. Therefore, only the locations of the first-order scattering are discussed. The average heights of the first-order scattering for profile (A) and profile (B) are given in Table 6 and Table 7, respectively. The first column from the left is the solar zenith angle; the second and third columns are the arithmatically averaged height h_a and variance Δh_a, respectively; the forth and fifth columns are the height average h_1 and variance Δh_1 obtained through weighting by the parallel component I_1 of the scattered light; the sixth and seventh columns are those weighted by the vertical component I_2; the eighth and nineth columns are those weighted by intensity $I=I_1+I_2$; and the tenth and eleventh columns are those weighted by $Q=I_2-I_1$. As all the first-order scattering events occur in the local zenith direction, the average directions are not shown in the tables. Since the arithmatical average represents the selected position of the first collision in the Monte-Carlo code, the difference between the arithmatical average and other averages reflects the efficiency of the code. But the arithmatical average itself has little to do with the contribution to measurements, therefore it is not discussed. Among other average heights, h_2, h_1 and h_Q are close to each other. h_1 is slightly different from them. This is because the value of I_2 is much greater than I_1; the average heights in column 6, 8 and 10 are mainly determined by the value of I_2. The following facts can clearly be seen from Table 6 and Table 7:

i. Most contributions come from the layer between 18 and 25 km when the solar zenith angle ranges from 92.6° to 93.9°. This result verifies the supposition of many researchers based on previous observations.

ii. When stratospheric aerosols increase by a factor of 10 (profile (B)), the average heights weighted by I_1 for solar zenith angles 86° and 88° change, but other average heights have no obvious variation. This is because the increase of I_1 resulting from the increase of multiple scattering. Nevertheless I_1 is still much less than I_2 so that it can not affect other average heights.

iii. The difference between the height weighted by I_1 and that weighted by I_2 can be as big as 5 km resulting from the difference between the aerosol scattering powers with respect to the parallel and vertical components.

iv. After the sun sets below the horizon, Δh tends to decrease with the increase of the solar depression angle. In other words, the contributing region is getting narrower. But the minimum of Δh is still 6 km which shows the rather low spatial resolution of this detecting method.

Table 6. The Average Heights (km) of the First-order Scattering and the Variances of the Heights for Profile (A)

θ	h_a	Δh_a	h_1	Δh_1	h_2	Δh_2	h_I	Δh_I	h_Q	Δh_Q
86.0	26.66	13.46	6.112	4.921	10.69	6.747	10.39	6.742	11.04	6.732
88.0	26.66	13.46	6.137	5.015	11.06	6.905	10.79	6.901	11.37	6.888
93.9	30.39	11.33	23.51	4.584	24.92	7.317	24.90	7.242	24.95	7.379
95.3	36.39	8.048	31.89	5.480	35.14	5.998	35.08	6.060	35.18	6.042
95.9	39.34	6.353	39.45	5.157	39.78	4.791	39.78	4.794	39.78	6.145

Table 7. The Average Heights (km) of the First-order Scattering and the Variances of the Heights for Profile (B)

θ	h_a	Δh_a	h_1	Δh_1	h_2	Δh_2	h_I	Δh_I	h_Q	Δh_Q
86.0	26.66	13.46	11.84	8.690	11.08	7.009	11.15	7.196	10.99	6.776
88.0	26.66	13.46	12.58	8.862	11.45	7.169	11.55	7.341	11.32	6.968
90.0	26.66	13.46	14.57	8.878	12.33	7.468	12.50	7.619	12.12	7.294
92.6	27.39	13.06	21.36	4.307	17.98	7.584	18.26	7.435	17.63	7.777
93.9	30.39	11.24	22.61	3.846	24.51	7.257	24.23	6.921	24.89	7.719
95.3	36.38	7.905	29.38	2.796	34.45	5.848	34.08	5.793	34.89	5.804

3. *Change of the Background Concentration of Stratospheric Aerosols*

Shown in Fig. 7 and Fig. 8 are the comparison of the simulated intensity and the degree of polarization with the measurements. It is clear that the simulated intensity coincides well with the measurements (Fig. 8). But the degree of polarization for profile (A) is considerably higher than those measurements from the region of $\theta > 90°$ when the degree of polarization corresponding to profile (B) is closer to the measurement data. According to a primary computation test, the uncertainty in the aerosol size distribution is unlikely the cause of such a great difference as between the result for profile (A) and the measurement data. Therefore, the discrepancy is mainly attributed to the enhancement of the aerosol scattering coefficient in the stratosphere which has resulted from the increase of the aerosol concentration. It follows that the background concentration of aerosols in the spring of 1977 was greater than that during the measurement by Junge et al. in 1959-1960, if we assume that there is no great change in the size distribution and refractive index of aerosols since the late 1950's. But the effect of the aerosol size distribution and refractive index on skylight should further be investigated in detail.

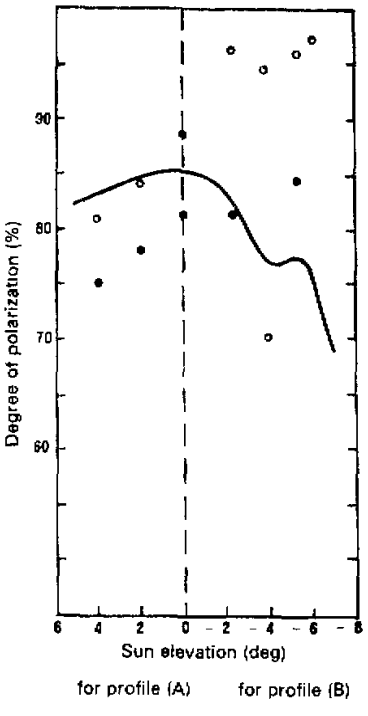

Fig. 7. The zenith polarization. Solid line is the observation; o the simulation for profile (A); • for profile (B).

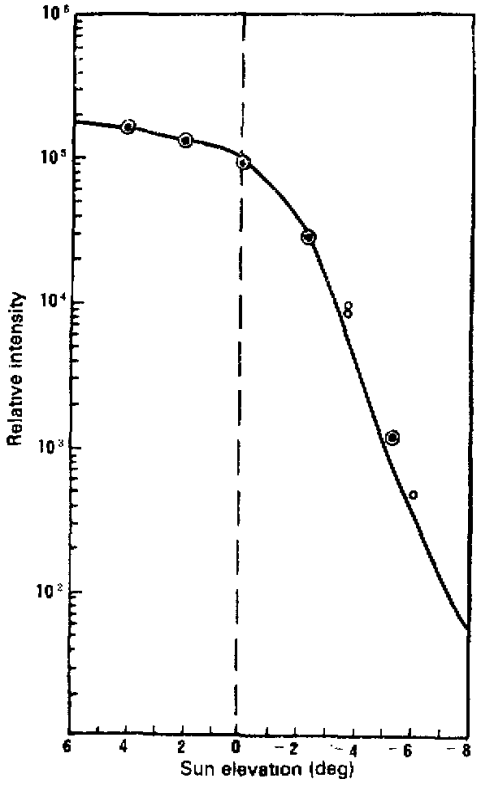

Fig. 8. The zenith intensity. The meanings of the symbols are the same as in Fig. 7.

There exists observed evidence for the higher background concentration in 1977. Bigg (1976) measured the size distribution and concentration of stratospheric particles with impactors carried on 35 Australian balloon flights along 34°S from May 1969 to April 1974. The observation showed that the particle concentration was about 0.4 particles/cm³ during this period except in 1971 when the concentration was less than 0.1 particles/cm³.

The dustsonde measurements made monthly by the University of Wyoming (Swissler et al., 1982) at Laramie (41.2°N, 105°W) during the period 1974–1980 showed that the stratospheric peak aerosol mixing ratio for particles with radii greater than 0.15 μm was 6 particles/mg for the period 1978–1979. This is equal to the peak concentration of 0.5 particles/cm³.

Hofmann and Rosen (1980) observed the maximum particle concentration for particles larger than 0.3 μm in diameter. The given concentration was 1 particle/cm³ in 1977, 0.8 particles/cm³ in 1978, and 0.7 particles/cm³ in 1979.

By contrast, the peak concentration measured by Junge et al. was about 0.1 particles/cm³.

Several minor volcanic eruption may be responsible for this increase of aerosol background concentration. For example, Fegley et al. (1980) reported an upper tropospheric

aerosol layer, which was thought to have originated at the volcano Nyiragonga (1.5°S, 29.2°E), appearing to penetrate the tropical tropopause in January 1977.

However, it remains unknown whether there is any anthropogenic effect on the increase and whether it has influenced the radiation and dynamics in the stratosphere.

IV. CONCLUSION

1. It can be found from the comparison between results for the background period and for the volcanic period that multiple scattering play completely different roles in the two cases. Single scattering approximation can be reasonably applied to the twilight problem during the background period, but higher order scattering must be taken into consideration after a violent volcanic eruption.

2. The characteristics of skylight during the twilight period can be simulated by using the Monte-Carlo code. However, there is slight discrepancy with measurements resulting from the uncertainty of the aerosol scattering coefficient, the difference in detecting manners of a lidar and a photometer and the assumption on the aerosol size distribution. The uncertainty in the aerosol scattering coefficient is likely the main cause of the discrepancy.

3. The background concentration of stratospheric aerosols has increased since the 1960's. It is necessary to study the cause of this increase and the potential effects on climate.

The authors wish to thank Dr. J. DeLuisi and Dr. K.L. Coulson for providing the lidar data and for helpful comments. Thanks are also due to Mrs. Zhang Daping for preparing some of the diagrams. This work was supported by the National Science Foundation under Grant R850294.

REFERENCES

Bigg E.K. (1976), Size Distributions of Stratospheric Aerosols and Their Variations with Altitude and Time, *J. Atmos. Sci.*, **33**:1080-1086.

Blattner W.G., H.G. Horak, D.G. Collins and M.B. Wells (1974), Monte Carlo Studies of the Sky Radiation at Twilight, *Appl. Opt.*, **13**:534-547.

Collins D.G. and M.B. Wells (1971), Computer Procedure for Calculating Time Dependent Light Scattering in Spherical-shell Atmosphere, Radiation Research Associate RRA-T7017.

Coulson K.L. (1980), Characteristics of Skylight at the Zenith during Twilight as Indicator of Atmospheric Turbidity. 1:Degree of polarization, *Appl. Opt.*, **19**:3469-3480.

Coulson K.L. (1981), Characteristics of Skylight at the Zenith during Twilight as Indicator of Atmospheric Turbidity. 2: Intensity and color ratio, *Appl. Opt.*, **20**:1516-1524.

Coulson K.L. (1983a), Effects of the El Chichon Volcanic Cloud in the Stratosphere on the Polarization of Light from the Sky, *Appl. Opt.*, **22**:1036-1049.

Coulson K.L. (1983b), Effects of the El Chichon Volcanic Cloud in the Stratosphere on the Intensity of Light from the Sky, *Appl. Opt.*, **22**:2265-2271.

Dave J.V. (1956), On the Intensity and Polarization of the Light from the Sky during Twilight, *Proc. Indian Acad. Sci. Sect A*43, No.6, 336-358.

DeLuisi J., T. DeFoor, K.Coulson and F. Fernald (1985), NOAA Data Report ERL ARL-5.

Divari N.B. (1967), Calculation of the Polarization of the Light of the Twilight Sky, *Atmos. Oceanic Phys.*, **3**:507-515.

Elterman L. (1968), UV, Visible and IR Attenuation for Altitude to 50 km, AFCRL-68-0153.

Fegley R.W. et al. (1980), Volcanic Contributions to the Stratospheric Sulfate Layer, *J. Appl. Meteor.*, **19**:683-690.

Hamill P., O.B. Toon and C.S. Kiang (1977), Microphysical Processes Affecting Stratospheric Aerosol Particles, *J. Atmos. Sci.*, **34**:1104.

Hofmann D.J. and J.M. Rosen (1980), Stratospheric Sulfuric Acid Layer: Evidence for an Anthropogenic Component, *Science*, **208**:1368-1370.

Handbook of Geophysics and Space Environments (1965), AFCRL.

Steinhorst G. (1977), Stratospheric Aerosol Concentration Determined by an Iterative Method from Twilight

Polarization Measurements, *Contri. Atmos. Phys.*, **50**:508–523.

Swissler T.J. et al. (1982), A Comparison of Lidar and Balloon-Borne Particles Counter Measurements of the Stratospheric Aerosol, *J. Atmos. Sci.*, **39**:909–916.

U.S. Standard Atmosphere (1976), National Oceanic and Atmospheric Administration, National Aeronautic and Space Administration, United States Air Force.